RESEARCH ARTICLE | DECEMBER 28 2017

Analysis of thermoelastic characteristics in a thick walled FGM cylinder FREE

A. N. M. Tanvir; Md. Didarul Islam; Faisal Ahmed

AIP Conf. Proc. 1919, 020030 (2017)
https://doi.org/10.1063/1.5018548

Analysis of Thermoelastic Characteristics in a Thick Walled FGM Cylinder

A. N. M. Tanvir[1, a)], Md. Didarul Islam[2, b)] and Faisal Ahmed[1, c)]

[1]*Bangladesh University of Engineering and Technology, Bangladesh*
[2]*University of Texas at El Paso, USA*

[a)]tanvir.10075@gmail.com
[b)]mislam13@miners.utep.edu
[c)]faisalme0710106@gmail.com

Abstract. This study is concerned with the behavior of stress and strain in a thick walled functionally graded material (FGM) cylinder under internal pressure. The incompatible eigenstrain and equivalent eigenstrain developed in the cylinder, are taken into account. As a demonstration, a TiC/Al_2O_3 FGM cylinder is considered and different components of stress and strain are presented in order to study the effects of internal pressure, temperature difference (between room and sintering temperature), cylinder wall thickness and material distribution. The numerical result presented here shows that the thermoelastic characteristic like stress and strain of an FGM cylinder is significantly influenced by some of the above-mentioned parameters and can be controlled by properly controlling these parameters.

INTRODUCTION

Functionally graded materials (FGMs) have outstanding advantages over homogeneous materials, alloys, and conventional composite materials. This is now variedly used in different applications like aerospace industries, nuclear power plants, and chemical industries. The most important characteristic of FGMs is their continuously varying material distribution which is advantageous for its application to adverse conditions like high temperature, high pressure, excessive wear, and corrosion while can maintain their structural properties along with machinability and thermal conductivity.

As, in adverse condition, stress is an important factor, many studies have been carried out regarding stresses in FGMs. Obata and Noda studied the steady state thermal stress field in a hollow circular cylinder and sphere whereas tried understanding the effect of volumetric ratio and porosity on the steady state stress [1]. Takezono et al. formulated analytically and numerically the thermal stress and deformation states for axisymmetrical shells of functionally graded material subjected to thermal loading due to a fluid and showed that the temperature distribution, stress distribution, and deformation in an FGM depends on composition and material distribution profile [2]. Recently, elastoplastic buckling behaviors of FGM cylinders under axial compression are investigated by Huaiwei and Qiang [3]. Thermal vibration behavior of functionally graded nanobeams exposed to various kinds of thermo-mechanical loading is studied by Ebrahimi and Reza Barati [4]. Jabbari et al. evaluated the mechanical and thermal stresses through direct solution of Navier equation in a FGM hollow cylinder under radially symmetric loads [5].

The present study focuses on the analysis of thermoelastic characteristics in a thick-walled FGM cylinder under internal pressure. This study is based on an approximation method developed by Afsar and sekin [6] to evaluate the stress intensity factors of edge cracks in FGM cylinders. In this approximation method, they have focused only on the fracture characteristics of the FGM cylinder. Elastic field, such as stress, strain, and displacement, was not

Proceedings of the 1st International Conference on Mechanical Engineering and Applied Science (ICMEAS 2017)
AIP Conf. Proc. 1919, 020030-1–020030-11; https://doi.org/10.1063/1.5018548
Published by AIP Publishing. 978-0-7354-1611-6/$30.00

analyzed by their developed method. The authors of the present study found that a part of the formulations of the approximation method developed by Afsar and sekin [6] could be useful in analyzing the elastic field in FGM or any nonhomogenous cylinder. Thus the objective of the present work is to apply the formulations of the approximation method to evaluate the thermoelastic characteristics of a thick walled FGM cylinder and examine the effect of internal pressure, temperature difference, material distribution, and cylinder wall thickness on the thermoelastic characteristics of the FGM cylinder.

MODELING OF THICK-WALLED FGM CIRCULAR CYLINDER

A thick-walled FGM circular cylinder with reference to the Cartesian coordinate system (x,y) and the polar coordinate system (r,θ) having the same origin located at the center of the cylinder is modeled as shown in Fig. 1.

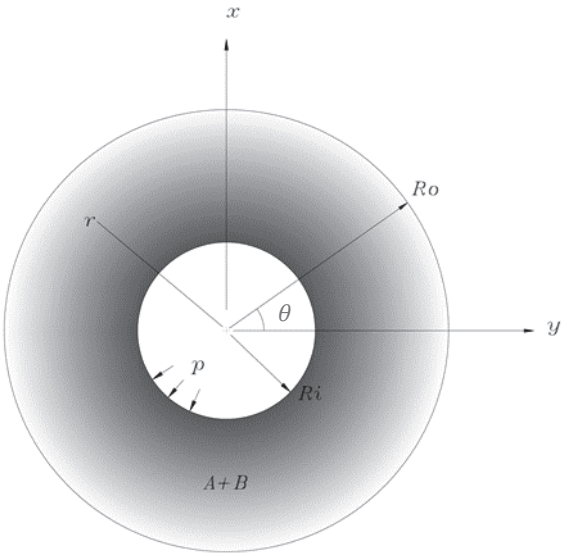

FIGURE 1. Modeling of a Thick-Walled FGM Cylinder.

The inner and outer radius of the cylinder is denoted by R_i and R_o respectively. The FGM cylinder consists of two constituent materials A and B. The volume fraction of the constituent materials varies only in the radial direction. Therefore, all the material properties of the FGM cylinder is the function of radius (r) only. For this modeling of the cylinder, an incompatible eigenstrain is developed due to nonuniform coefficient of thermal expansion (CTE) and thermal gradient. The incompatible eigenstrain is defined by

$$\varepsilon^*(r) = -\alpha(r)\Delta T \tag{1}$$

Where α is the coefficient of thermal expansion of the FGM cylinder and ΔT is the difference between the sintering temperature and room temperature. As the material of the FGM cylinder is assumed to be isotropic, the shear component of the incompatible eigenstrain vanishes and the normal components become equal. The analysis is carried out under plain strain condition (ε_z=0).

Equivalent Eigenstrain Simulating Nonhomogeneous Material Properties of Thick-Walled FGM Cylinders

The FGM cylinder is divided into n number of layers of infinitesimal thickness and only one half is shown in Fig.2. The inner and outer radii of the i^{th} layer are denoted by r_{i-1} and r_i respectively where r_o=R_i and r_i=R_n. The pressure at the inner and the outer surfaces of the i^{th} layer of the layered FGM cylinder are denoted by P_{i-1}^f and P_i^f ,

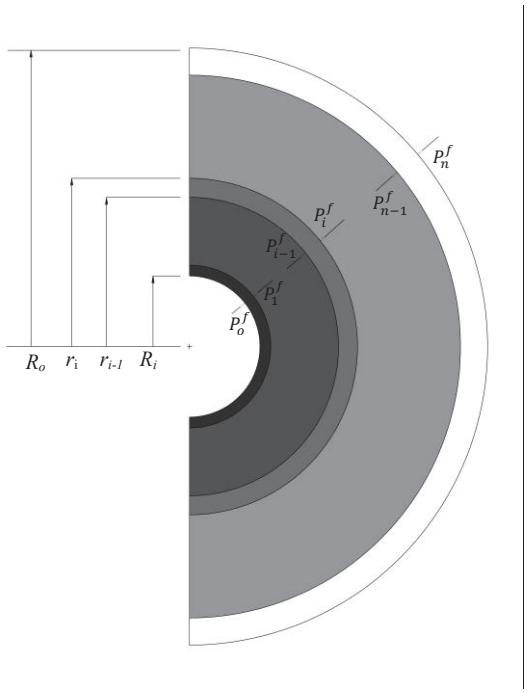

FIGURE 2. FGM cylinder with infinite homogenous layers.

which are the resultant of pressures due to applied internal pressure p and incompatible eigenstrain ε^*. The pressure at the inner and the outer surfaces of the i^{th} layer of the homogenized FGM cylinder are denoted by P_{i-1}^h and P_i^h. The components of strain field in the FGM cylinder is derived by Afsar and sekin [6].

Resultant radial strain,

$$\varepsilon_{r,e}^i = \frac{(1+\nu_i)(1-2\nu_i)}{E_i(1-c_i^2)}[(c_i^2P_{i-1}^f - P_i^f) - \frac{c_i^2}{(1-2\nu_i)} \times \frac{r_i^2}{r^2}(P_{i-1}^f - P_i^f)] - \frac{(1+\nu_0)(1-2\nu_0)}{E_0(1-c_i^2)}[(c_i^2P_{i-1}^h - P_i^h) - \frac{c_i^2}{(1-2\nu_0)} \times$$
$$\frac{r_i^2}{r^2}(P_{i-1}^h - P_i^h)] + \frac{1}{E_0(1-c_i^2)}[c_i^2(1-\frac{r_i^2}{r^2})(P_{i-1}^h - P_{i-1}^f) - (1-c_i^2\frac{r_i^2}{r^2})(P_i^h - P_i^f)] - \frac{\nu_0}{E_0(1-c_i^2)}[c_i^2(1+\frac{r_i^2}{r^2})(P_{i-1}^h - P_{i-1}^f) - \quad (2)$$
$$(1+c_i^2\frac{r_i^2}{r^2})(P_i^h - P_i^f)] - \frac{2\nu_0}{E_0(1-c_i^2)}[\nu_0(c_i^2P_{i-1}^h - P_i^h) - \nu_i(c_i^2P_{i-1}^f - P_i^f)] + \frac{\varepsilon_i^*}{E_0}(E_0\nu_i - E_i\nu_0)$$

Resultant circumferential strain,

$$\varepsilon_{\theta,e}^i = \frac{(1+\nu_i)(1-2\nu_i)}{E_i(1-c_i^2)}[(c_i^2P_{i-1}^f - P_i^f) - \frac{c_i^2}{(1-2\nu_i)} \times \frac{r_i^2}{r^2}(P_{i-1}^f - P_i^f)] - \frac{(1+\nu_0)(1-2\nu_0)}{E_0(1-c_i^2)}[(c_i^2P_{i-1}^h - P_i^h) - \frac{c_i^2}{(1-2\nu_0)} \times$$
$$\frac{r_i^2}{r^2}(P_{i-1}^h - P_i^h)] + \frac{1}{E_0(1-c_i^2)}[c_i^2(1+\frac{r_i^2}{r^2})(P_{i-1}^h - P_{i-1}^f) - (1+c_i^2\frac{r_i^2}{r^2})(P_i^h - P_i^f)] - \frac{\nu_0}{E_0(1-c_i^2)}[c_i^2(1-\frac{r_i^2}{r^2})(P_{i-1}^h - P_{i-1}^f) - \quad (3)$$
$$(1-c_i^2\frac{r_i^2}{r^2})(P_i^h - P_i^f)] - \frac{2\nu_0}{E_0(1-c_i^2)}[\nu_0(c_i^2P_{i-1}^h - P_i^h) - \nu_i(c_i^2P_{i-1}^f - P_i^f)] + \frac{\varepsilon_i^*}{E_0}(E_0\nu_i - E_i\nu_0)$$

Resultant axial strain,

$$\varepsilon_{z,e}^i = \frac{2}{E_0(1-c_i^2)}[\nu_0(c_i^2P_{i-1}^h - P_i^h) - \nu_i(c_i^2P_{i-1}^f - P_i^f)] - \frac{2\nu_0}{E_0(1-c_i^2)}[c_i^2(P_{i-1}^h - P_{i-1}^f) - (P_i^h - P_i^f)] + \frac{\varepsilon_i^*}{E_0}(E_0\nu_i - E_i\nu_0) \quad (4)$$

where, c_i is the ratio of inner to outer radius (r_{i-1}/r_i) of a nonhomogenous layer in the FGM cylinder. The value of P_{i-1}^f and P_i^f can be obtained by linearly solving equation (5) to (8) provided by Afsar and sekin [6] given below

$$\delta_{i,i-1}^f r_{i-1} p_{i-1}^f + \delta_{i,i}^f r_i p_i^f + \delta_{i,i+1}^f r_{i+1} p_{i+1}^f = 0 \quad (5)$$

$$\delta_{i,i-1}^{f} r_{i-1} p_{i-1}^{*,f} + \delta_{i,i}^{f} r_i p_i^{*,f} + \delta_{i,i+1}^{f} r_{i+1} p_{i+1}^{*,f} = r_i[(1+\nu_{i+1})\varepsilon_{i+1}^{*} - (1+\nu_i)\varepsilon_i^{*}] \tag{6}$$

$$p_0^{f} = p, p_n^{f} = p_0^{*,f} = p_n^{*,f} = 0; \tag{7}$$

$$P_i^{f} = p_i^{f} + p_i^{*f} \tag{8}$$

where, $i = 1,2,3,....,n-1$;

$$\delta_{i,i-1}^{f} = \frac{2c_i(1-\nu_i^2)}{E_i(1-c_i^2)};$$

$$\delta_{i,i}^{f} = -\frac{(1+\nu_i)}{E_i(1-c_i^2)}\{1-2\nu_i+c_i^2\} - \frac{(1+\nu_{i+1})}{E_{i+1}(1-c_{i+1}^2)}\{c_{i+1}^2 - 2\nu_{i+1}c_{i+1}^2 + 1\},$$

;

$$\delta_{i,i+1}^{f} = \frac{2c_{i+1}(1-\nu_{i+1}^2)}{E_{i+1}(1-c_{i+1}^2)};$$

where, p_i^{f} and p_i^{*f} are the pressure due to applied internal pressure and incompatible eigenstrain respectively. P_{i-1}^{h} and P_i^{h} can be obtained by linearly solving equation (9) to (12) developed by Afsar and sekin [6].

$$\delta_{i,i-1}^{h} r_{i-1} p_{i-1}^{h} + \delta_{i,i}^{h} r_i p_i^{h} + \delta_{i,i+1}^{h} r_{i+1} p_{i+1}^{h} = 0 \tag{9}$$

$$\delta_{i,i-1}^{h} r_{i-1} p_{i-1}^{*h} + \delta_{i,i}^{h} r_i p_i^{*,h} + \delta_{i,i+1}^{h} r_{i+1} p_{i+1}^{*,h} = r_i(1+\nu_0)(\varepsilon_{i+1}^{*} - \varepsilon_i^{*}) \tag{10}$$

$$p_0^{h} = p, p_n^{h} = p_0^{*,h} = p_n^{*,h} = 0; \tag{11}$$

$$P_i^{f} = p_i^{f} + p_i^{*f} \tag{12}$$

where, $i = 1,2,3,....,n-1;$

$$\delta_{i,i-1}^{h} = \frac{2c_i(1-\nu_0^2)}{E_0(1-c_i^2)};$$

$$\delta_{i,i}^{h} = -\frac{(1+\nu_0)}{E_0}\left[\frac{1}{(1-c_i^2)}\{1-2\nu_0+c_i^2\} - \frac{1}{(1-c_{i+1}^2)}\{c_{i+1}^2 - 2\nu_0 c_{i+1}^2 + 1\}\right];$$

$$\delta_{i,i+1}^{h} = \frac{2c_{i+1}(1-\nu_0^2)}{E_0(1-c_{i+1}^2)};$$

where, p_i^{h} and p_i^{*h} are the pressure due to applied internal pressure and incompatible eigenstrain respectively in the homogenized FGM cylinder. Stress components are thus obtained by Afsar and sekin [6].

Resultant radial stress field,

$$\sigma_r^{h} = \frac{R_i^2 p}{R_0^2 - R_i^2}\left(1 - \frac{R_0^2}{r^2}\right) + \frac{E_0}{(1-\nu_0)}\left[-\frac{1}{r^2}\int_{R_i}^{r} \varepsilon^{*} r dr + \left(1 - \frac{R_i^2}{r^2}\right)\frac{1}{(R_0^2 - R_i^2)}\int_{R_i}^{R_0} \varepsilon^{*} r dr\right]$$
$$+ \frac{E_0}{2(1-\nu_0^2)}\left[-\frac{1}{r^2}\int_{R_i}^{r} r\left(\varepsilon_r^{e} + \varepsilon_\theta^{e} + 2\nu_0\varepsilon_z^{e}\right)dr + \int_{R_i}^{r}\frac{1}{r}\left(\varepsilon_r^{e} - \varepsilon_\theta^{e}\right)dr + C\left(1 - \frac{R_i^2}{r^2}\right)\right] \tag{13}$$

Resultant circumferential stress field,

$$\sigma_\theta^{h} = \frac{R_i^2}{R_0^2 - R_i^2}\left(1 + \frac{R_i^2}{r^2}\right) + \frac{E_0}{(1-\nu_0)}\left[-\varepsilon^{*} + \frac{1}{r^2}\int_{R_i}^{r} r\varepsilon^{*} dr + \frac{1}{(R_0^2 - R_i^2)}\left(1 + \frac{R_i^2}{r^2}\right)\int_{R_i}^{R_0} r\varepsilon^{*} dr\right] +$$
$$\frac{E_0}{2(1-\nu_0^2)}\left[-2\left(\varepsilon_\theta^{e} + \nu_0\varepsilon_z^{e}\right) + \frac{1}{r^2}\int_{R_i}^{r} r\left(\varepsilon_\theta^{e} + \varepsilon_r^{e} + 2\nu_0\varepsilon_z^{e}\right)dr + \int_{R_i}^{r}\frac{1}{r}\left(\varepsilon_r^{e} - \varepsilon_\theta^{e}\right)dr + C\left(1 + \frac{R_i^2}{r^2}\right)\right] \tag{14}$$

Resultant Axial Stress field,

$$\sigma_z^{h} = \frac{2\nu_0 R_i^2 p}{R_0^2 - R_i^2} + \frac{E_0\nu_0}{1-\nu_0}\left\{-\varepsilon^{*} + \frac{2}{R_0^2 - R_i^2}\int_{R_i^2}^{R_0^2} r\varepsilon^{*} dr\right\} + \frac{E_0\nu_0}{1-\nu_0^2}\left[-\left(\varepsilon_\theta^{e} + \nu_0\varepsilon_z^{e}\right) + \int_{R_i}^{r}\frac{1}{r}\left(\varepsilon_r^{e} - \varepsilon_\theta^{e}\right)dr + C\right] - E_0\left(\varepsilon^{*} + \varepsilon_z^{e}\right) \tag{15}$$

where, $C = \frac{1}{R_0^2 - R_i^2}\left\{\int_{R_i}^{R_0} r(\varepsilon_r^e + \varepsilon_\theta^e + 2\nu_0\varepsilon_z^e)dr - R_0^2\int_{R_i}^{R_0}\frac{1}{r}\left(\varepsilon_r^e - \varepsilon_\theta^e\right)dr\right\}$

α is the CTE of the FGM cylinder. The CTE can be obtained by using the mixture rule formula developed by Nan C-W, Yan R-Z, Zhong L-M [7] for two different materials. It can be obtained by first finding shear modulus of elasticity μ and bulk modulus of elasticity K using following relations-

$$V_A\frac{K_A - K}{3K_A + 4\mu} + V_B\frac{K_B - K}{3K_B + 4\mu} = 0; \tag{16}$$

$$V_A\frac{\mu_A - \mu}{\mu_A + Y} + V_B\frac{\mu_B - \mu}{\mu_B + Y} = 0; \tag{17}$$

$$Y = \frac{\mu(9K + 8\mu)}{6K + 12\mu}; \tag{18}$$

where Y is the young's modulus of elasticity. The subscripts A and B represent the respective material properties for respective volume fractions of the materials. Non-subscripted variables are used to denote the properties of the FGM homogenized cylinder. Then Young's modulus E, Poisson's ratio ν, and coefficient of thermal expansion α are calculated by using the expressions-

$$E = \frac{9K\mu}{(3K + \mu)},\ \nu = \frac{E}{2\mu} - 1 \tag{19}$$

$$\alpha = V_A\alpha_A\frac{K_A(3K + 4\mu)}{K(3K_A + 4\mu)} + V_B\alpha_B\frac{K_B(3K + 4\mu)}{K(3K_B + 4\mu)} \tag{20}$$

RESULTS AND DISCUSSION

Numerical results are obtained for TiC/Al_2O_3 FGM cylinders in which TiC and Al_2O_3 represent the materials A and B, respectively. The mechanical and thermal properties of TiC and Al_2O_3 are shown in Table 1.

TABLE 1. Material properties of the constituent materials

Material	Young's Modulus, Y (GPa)	Shear Modulus μ (GPa)	Poisson's Ratio, ν	Coefficient of Thermal Expansion, α ($°C^{-1}$)
TiC (A)	462	194.12	0.19	7.4×10^{-6}
Al_2O_3 (B)	380	150.79	0.26	8×10^{-6}

Material distribution of the circular homogenized FGM cylinder is assumed using three equations at random.

$$V_B = 1 - \frac{r - R_i}{R_0 - R_i} \tag{21}$$

$$V_B = 1 - \left(\frac{r - R_i}{R_0 - R_i}\right)^2 \tag{22}$$

$$V_B = 1 - \sqrt{\left(\frac{r - R_i}{R_0 - R_i}\right)} \tag{23}$$

$$V_A + V_B = 1 \tag{24}$$

Equation (21), (22), and (23) will be addressed as profile-1, profile-2, and profile-3 respectively in the following section. V_A and V_B denote the volume fraction of the TiC and Al_2O_3 in the FGM cylinder at a radius *(r)* respectively. Below is the graphical representation of material distribution profiles used for the analysis (Fig. 3.)-

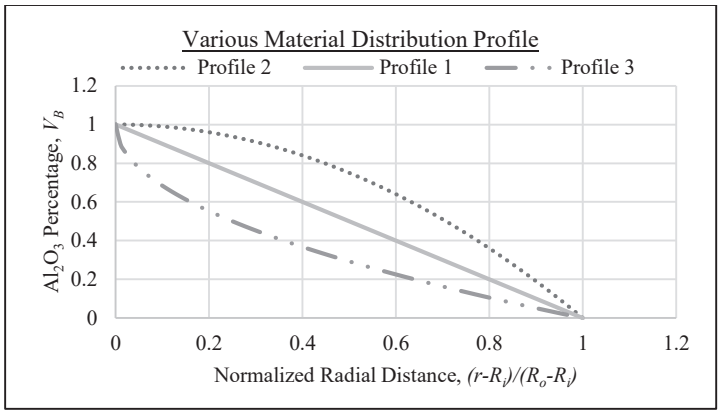

FIGURE 3. Prescribed material distribution.

For analyzing the behavior of stress and strains, equations 1-20 are simulated in a simple Matlab code. The numerical results are plotted. Performance parameters considered are internal pressure (P_i), the difference between room temperature and sintering temperature (ΔT), and the ratio of outer and inner radius (R_0/R_i). The internal pressure applied to the FGM circular cylinder are 100MPa, 300MPa, and 500MPa. Difference between room temperature and sintering temperature considered are 400℃, 700℃, 1000℃. Ratio of outer to inner radius considered are 2, 3, and 4. Internal radius (R_i) is maintained constant at 0.5m, but outer radius (R_o) is varied to change the radius ratio. Stresses and strains are plotted against normalized radius $(r-R_i)/(R_0-R_i)$ to obtain the behavior of radial, circumferential, and axial stress and strain under different material distributions, temperature difference, pressure, and thickness of the cylinder. To have an isolated behavior throughout the circular cylinder 18 sets of evaluated data are chosen and are plotted keeping at least two performance parameter constant in one plot.

Behavior of Radial Stress

Radial stress decreases with increasing internal pressure and thickness of the cylinder keeping other parameters constant (Fig. 4(a) and 4(c)). For increasing temperature difference radial stress increases in the FGM cylinder (Fig. 4(b)).

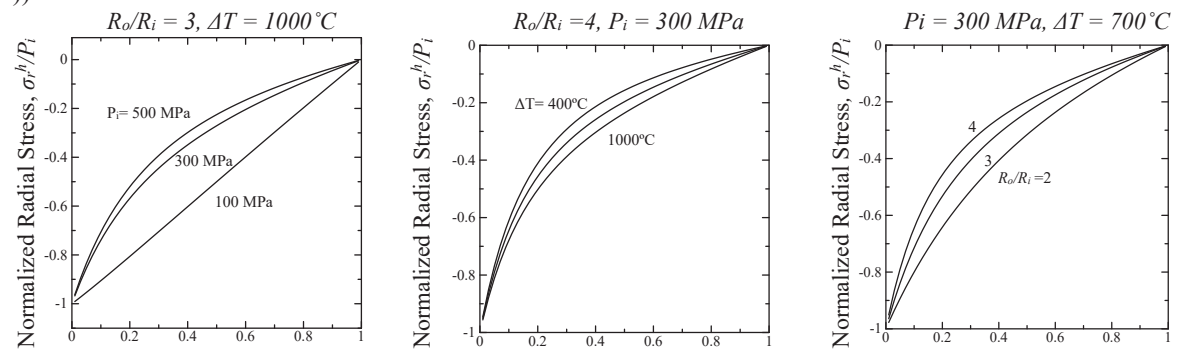

FIGURE 4. Behavior of radial stress as a function of normalized distance for varying (a) internal pressure (b) temperature difference (c) cylinder thickness.

Behavior of Circumferential Stress

Circumferential stress varies more in the high temperature and low pressure case (Fig. 5(a)). By increasing internally applied pressure, variation in stress value and direction can be both altered significantly. For varying temperature difference (ΔT) circumferential stress decreases first for the inner portion of the cylinder. For lower

temperature, after reaching a lowest value it increases as the radius increases, but for higher temperature, after reaching the lowest value it becomes almost stable and constant (Fig. 5(b)). For the lowest pressure (100MPa) and highest temperature (1000˚C) observed the circumferential stress behaves linearly (Fig. 5(a)). For changing ΔT and p_i stress for different condition become equal at a particular point on the non-dimensional radial direction (approximately at 0.46). Circumferential stress decreases as the thickness of the cylinder increases (Fig. 5(c)).

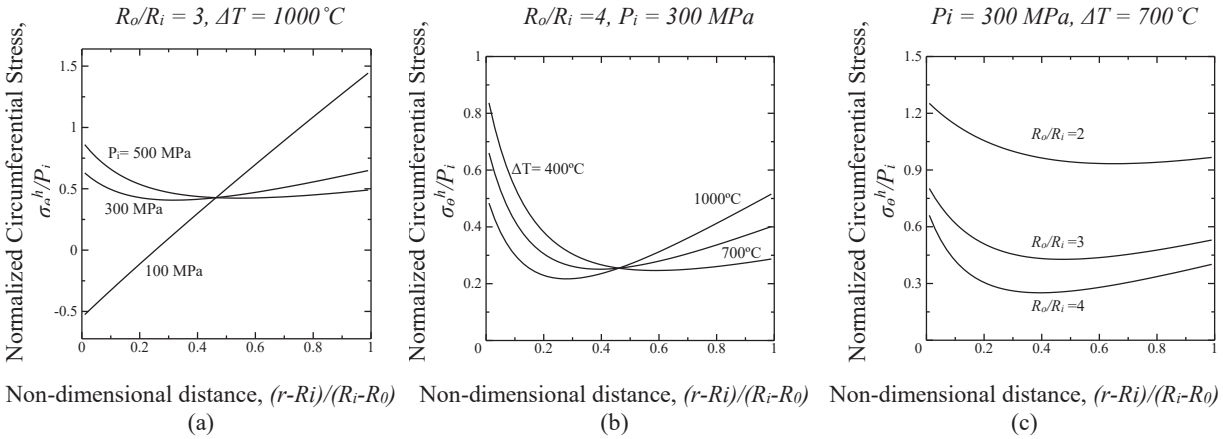

FIGURE 5. Behavior of circumferential stress as a function of normalized distance for varying (a) internal pressure (b) temperature difference (c) cylinder thickness.

Behavior of Axial Stress

Axial stress always behaves linearly for varying all the parameters. The magnitude of axial stress is higher compared to other stresses (radial and circumferential) which is due to the effect of very high stress developed due to eigenstrain. Due to increasing internal pressure axial stress decreases (Fig. 6(a)). Due to increasing ΔT and R_o/R_i axial stress increases. But for the temperature variation degree of increase is much higher compared to increase in thickness (Fig. 6(b) and 6(c)).

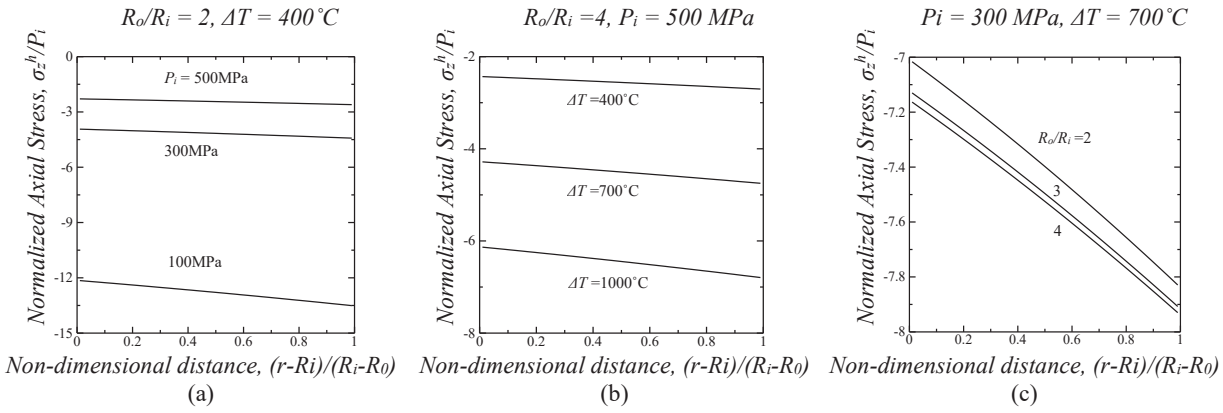

FIGURE 6. Behavior of axial stress as a function of normalized distance for varying (a) internal pressure (b) temperature difference (c) cylinder thickness.

Behavior of Stress for Different Material Distributions

Material distribution of the FGM circular cylinder affects stresses in the cylinder. Here we assumed three profiles of material distribution- profile 1, profile 2 and profile 3 (Equation 21, 22, 23). The three profiles are compared in the same graph to observe the effect. Radial stress doesn't change significantly due to change in

material distribution (Fig 7(a)). For circumferential stress profile 2 and 3 give almost same value of stress. Profile-1 on the other hand yields a different curve (Fig 7(b)). Profile 2 and 3 give almost same terminal value but different values in the central portion of the cylinder wall for axial stress, whereas, profile 1 gives a linear curve (Fig 7(c)). For eigenstress along the radial direction, higher stress is observed in profile 2 and 3 material distribution. Profile 1 distribution yields lower stress comparatively.

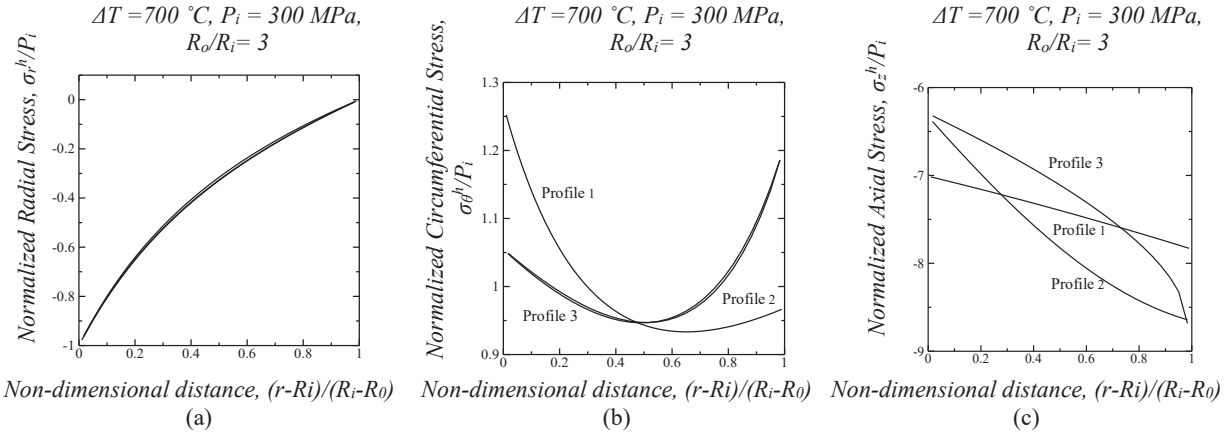

FIGURE 7. Behavior of various stress components as a function of normalized distance for varying material distribution (a) radial stress, (b) circumferential stress, (c) axial stress.

Behavior of Radial Strain

Varying internal pressure keeping temperature and radius ratio constant has no significant effect on the radial strain. For lower internal pressure we observed little increase in strain (Fig 8(a)). It varies significantly only in the case of temperature variation and keeping other parameters constant (Fig 8(b)). This is the effect of eigenstrain in the radial direction. Varying radius ratio keeping temperature and pressure constant has no significant effect on the radial strain. For higher thickness, we get little increase in strain (Fig 8(c)). Radial strain increases with increase in radius along the thickness of the FGM circular cylinder.

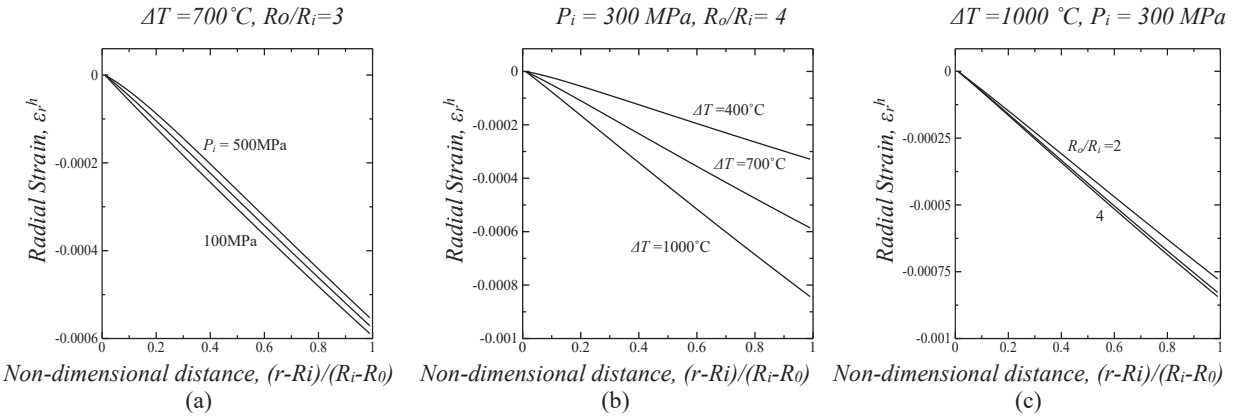

FIGURE 8. Behavior of radial strain as a function of normalized distance for varying (a) internal pressure (b) temperature difference (c) cylinder thickness.

Behavior of Circumferential Strain

Varying internal pressure with keeping temperature and radius ratio constant has no significant effect on the circumferential strain. For higher internal pressure strain increases a little (Fig 9(a)). Circumferential strain from the inner radius to outer radius increases with increasing temperature difference keeping internal pressure and radius ratio constant. Higher range of variation can be observed in the FGM with the higher temperature difference. This is mainly due to the effect of eigenstrain (Fig 9(b)). In thicker walled cylinder we observed slightly higher circumferential strain (Fig 9(c)).

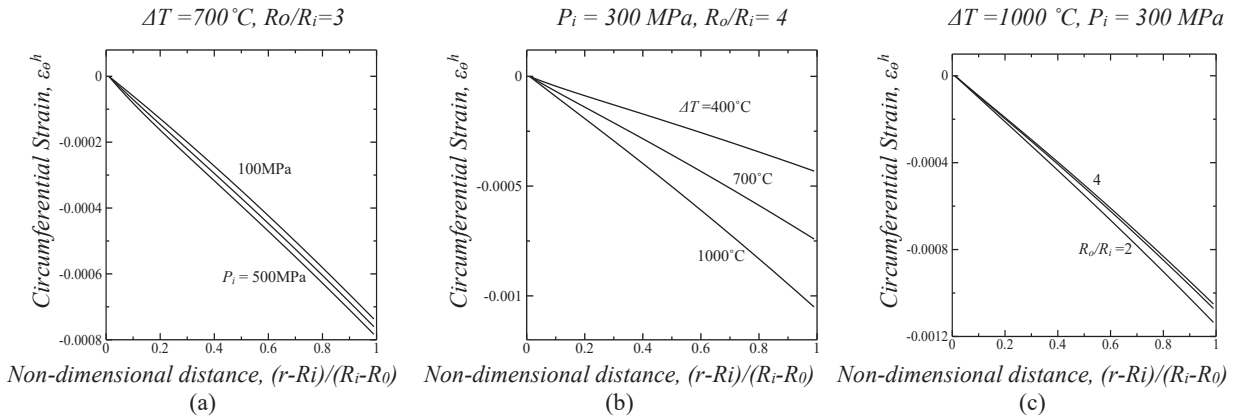

FIGURE 9. Behavior of circumferential strain as a function of normalized distance for varying (a) internal pressure (b) temperature difference (c) cylinder thickness.

Behavior of Axial Strain

For lower internal pressure little increase in axial strain is seen in Fig. 10(a). This is due to the fact of stress and strain at axial direction being mostly dependent on temperature. Little temperature change gives higher strain. The slope of the higher temperature curve is higher than the curve obtained from lower temperature observation (Fig. 10(b)). This is the effect of eigenstrain along the axial direction. Varying thickness keeping temperature and pressure constant has no significant effect on the axial strain. For lower radius ratio we get a very slight increase in strain (Fig. 10(c)). Strain increases with increase in radius along the thickness of the FGM circular cylinder.

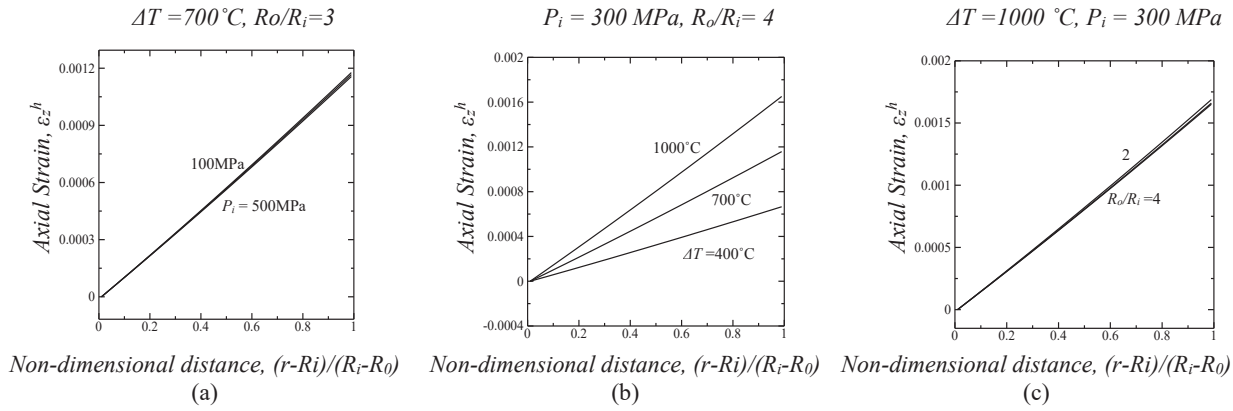

FIGURE 10. Behavior of axial strain as a function of normalized distance for varying (a) internal pressure, (b) temperature difference, (c) cylinder thickness.

Behavior of Strains for Different Material Distributions

Profile 1 gives a linear curve of the radial strain. But profile 2 and 3 distribution have different behavior. Among all the distributions, profile 3 provides the lowest strain ranging from positive to negative along the radius of the cylinder for radial and circumferential strain (Fig 11(a) and (b)). Along the thickness, zero strain can be observed at an intermediate point of the FGM cylinder for profile 2 and 3, which is at the innermost point for material distribution profile 1. Axial strain increases with the normalized distance in all the material distribution profiles unlike radial and circumferential strain (Fig 11(c)).

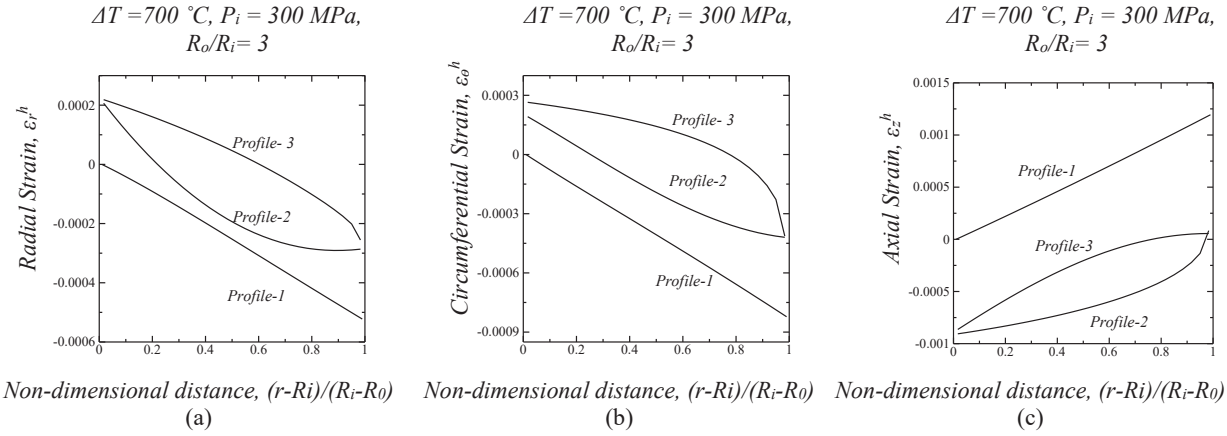

FIGURE 11. Behavior of various strain as a function of normalized distance for varying material distribution (a) radial strain, (b) circumferential strain, (c) axial strain.

CONCLUSIONS

An approximation method for evaluating stress intensity factor for edge cracks in a thick walled FGM cylinder has been rigorously studied. Formulation of the approximation method has been applied for the evaluation and analysis of various strains related in a thick walled FGM cylinder subjected to an internal pressure. The numerical results obtained for a TiC/Al_2O_3 FGM cylinder are presented in the form of graphs. It is found that the strains of an FGM cylinder are not significantly influenced by internal pressure and cylinder wall thickness. But temperature difference between room and sintering temperature and material distribution profile has significant effect on the radial, circumferential, eigenstrain, and axial strain. Thus the strain components can be controlled by properly controlling temperature and material distribution profile only. Failure analysis, using more materials in the simulation, and using more internal pressure and temperature range can be useful for using this study in practical purposes like designing a combustion chamber of a gas turbine or a cylinder of a diesel engine.

AKNOWLEDGEMENTS

The authors of this paper are grateful to Dr. A. M. Afsar, Professor, Department of Mechanical Engineering, Bangladesh University of Engineering and Technology, for his contribution and supervision throughout the whole research.

REFERENCES

1. Yooshihiro Obata and Naotake Noda, “Steady Thermal Stresses in a Hollow Circular Cylinder and a Hollow Sphere of a Functionally Gradient Material,” in *Journal of Thermal Stresses* 17, London, 1994 (Taylor & Francis, London, 1994), pp. 471-487.

2. Shigeo Takezono, Katsumi Tao, Eijiroh Inamura, and Masahiro Inoue, “Thermal Stress and Deformation in Functionally Graded Material Shells of Revolution under Thermal Loading due to Fluid,” in *JSME International Journal* 39, 1996 (The Japan Society of Mechanical Engineers, Tokyo, 1996), pp. 573-581.
3. Huaiwei Huang and Qiang Han, “Elastoplastic buckling of axially loaded functionally graded material cylindrical shells,” in *International Journal of Composite Structures* 117, 2014, pp. 135-142.
4. Ebrahimi, Farzad and Mohammad Reza Barati, “Vibration analysis of nonlocal beams made of functionally graded material in thermal environment,” in *European Physical Journal Plus* 131, 2016 (Springer Publishing, New York, 2016), article 279.
5. M. Jabbaria , S. Sohrabpourb , M.R. Eslami, “Mechanical and thermal stresses in a functionally graded hollow cylinder due to radially symmetric loads,” in *International Journal of Pressure Vessels and Piping* 79, 2002, pp. 493–497.
6. Afsar, A.M. and H. Sekine. “Optimum material distributions for prescribed apparent fracture toughness in thick-walled FGM circular cylinders,” in *International Journal of Pressure Vessels and Piping* 78.7, 2001, pp. 471-484.
7. Nan C-W, Yuan R-Z, Zhang L-M, “The Physics of metal/ceramic functionally gradient materials,” in *Ceramic transaction, functionally gradient materials* 34, 1993 (The American Ceramic Society, Westerville, Ohio, 1993), pp. 75-82.